Magnetic Domain Wall Propagation unto the Percolation Threshold across a Pseudorectangular Disordered Lattice

J. P. Attané,[1] Y. Samson,[1,*] A. Marty,[1] J. C. Toussaint,[2] G. Dubois,[3] A. Mougin,[3] and J. P. Jamet[3]

[1]*DRFMC / CEA Grenoble, 17 avenue des Martyrs, 38054 Grenoble Cedex 9, France*

[2]*Laboratoire Louis Néel / CNRS, 25 avenue des Martyrs, BP 166, 38042 Grenoble, France*

[3]*Laboratoire de Physique des Solides, UMR CNRS 8502, Université Paris Sud, 91405 Orsay, France*

(Received 4 June 2004; published 13 December 2004)

The reversal process of thin FePt/Pt(001) layers with perpendicular magnetization was observed by magnetic imaging techniques. Reversal occurs through domain wall propagation across a strongly disordered rectangular lattice of linear anisotropy defects. Micromagnetic simulations of domain wall pinning allowed deriving an analytical model of the reversal process unto percolation threshold. Quantitative agreement is found between the calculated and experimental fractal dimension of the reversed domain.

DOI: 10.1103/PhysRevLett.93.257203 PACS numbers: 75.60.Ch, 75.60.Jk

In thin magnetic layers, domain wall shape and motion are usually driven by the competition between the elastic stiffness of the wall and the local pinning. The former tends to minimize the wall length whereas the latter induces roughening, through local fluctuations of the wall energy linked to the structural disorder. These processes are of the highest interest as their study belongs to a fascinating and rich branch of modern physics; indeed, the same competition arises in as diverse phenomena as the fluid invasion of porous media [1], the dynamic of vortex lines in type-II superconductors [2], etc. In thin films with perpendicular magnetization, the demagnetizing field, due to long range interactions, tends to divide the system into small domains of opposite magnetization. In systems that combine perpendicular anisotropy and disorder, many studies revealed fractal geometries of magnetic domains [3–5] or fractal wall configurations [4,6]. Theoretical papers, mainly based on Monte Carlo simulations, explored the required set of parameters (disorder, thermal activation, demagnetizing field, wall energy) to obtain fractal patterns. Lyberatos underlined the need for spatial disorder [7], often induced by local unknown structural defects such as grain boundaries [8], that was accounted for in simulations by the distribution of one of the parameters: anisotropy [9], domain wall coercivity [10], coercive field [4,7,11], size of the crystallites [12]. In this Letter, we focus on domain wall interaction with strongly pinning linear defects in FePt thin films with perpendicular anisotropy. These defects (namely microtwins, see [13,14]) are introduced by strain relaxation processes during the layer growth on Pt(001). During magnetization reversal, at small scales, the domain wall adopts the shape of the defect [15] (another case of pinning by elongated defects has been provided by steps in Pt/Co/Pt trilayers [16]). At large scales, we discovered that this does not prevent the onset of fractal configurations. We propose a detailed micromagnetic analysis of the interaction between the domain and the structural defect. This deep understanding of the source of disorder warrants an analytical model for the beginning of the magnetization reversal. Originally, it reproduces the observed fractal magnetic pattern of the reversed domains at large scale and allows for a quantitative prediction of the fractal dimension.

We used 40 nm thin FePt(001) layers grown by molecular beam epitaxy, as such layers exhibit unique features of interest. First, a huge magnetocrystalline anisotropy, about $5 \times 10^6\ \mathrm{J\,m^{-3}}$, is obtained through uniaxial chemical ordering of the alloy within the $L1_0$ structure [15]. The remnant hysteresis loop obtained after switching off the magnetic field for each measure [see Fig. 1(a)] allows the observation of intermediate states of the reversal process at zero applied field. For magnetic force microscopy (MFM) and magneto-optical microscopy, the sample was saturated in a large positive field (1.2 T), next decreased down to a given negative value. The field cancellation freezes the reversal process, allowing imaging. Second, the microtwins [13,14] provide

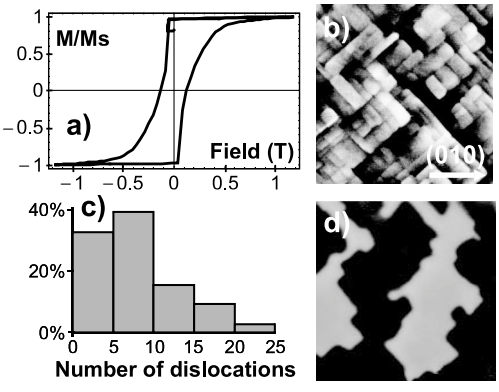

FIG. 1. For a FePt(40 nm)/Pt(001) layer: (a) Hysteresis loop. (b) 1 μm × 1 μm AFM image. (c) Probability density of the number of constitutive dislocations per microtwin. (d) 2 μm × 2 μm MFM image; the reversed domain is the dark one.

 © 2004 The American Physical Society

strong pinning positions for the domain walls [15]. They relax the tensile misfit (~1%) between the chemically ordered alloy and the Pt(001) substrate and result from the gliding of $1/6\langle 112\rangle$ partial dislocations on adjacent (111) atomic planes. These almost bidimensional defects are up to a few nm wide (up to 20–25 piled dislocations), a few 100 nm long, and extend from the bottom FePt/Pt interface to the upper Pt capping. Inside the microtwins, $L1_0$ order is also present. The magnetocrystalline anisotropy axis is oriented at 70.52° from the perpendicular to the sample surface, as expected from the mechanism of formation of the microtwins and observed by high resolution transmission electron microscopy (TEM) images. The surface step left at the emergence of the microtwin (along one of the $\langle 110\rangle$ direction) can be easily localized by atomic-force microscopy (AFM) [Fig. 1(b)] [13]. Indeed, images reveal a nanostructuration of the FePt layer within a pseudorectangular lattice, where the average distance between neighboring defects is 70 nm. The height of the surface step depends on the number of constitutive dislocations [Fig. 1(c), statistic from a few images]. At small scale, MFM images indicate that the domain walls are along either the [110] or $[1\bar{1}0]$ direction [Fig. 1(d)], and always located on a microtwin [15]. The resolution of the MFM technique (~30 nm) does not allow one to determine if propagation of a domain wall has been obstructed by a microtwin (corresponding thus to an energy barrier) and is jammed here by the pressure of the demagnetizing field, or if the domain wall is pinned on the microtwin (corresponding thus to an energy well).

The answer is provided by micromagnetic simulations, which demonstrate in cross section how the local pinning occurs. Indeed, thanks to the particular properties of the microtwins, the simulation does not require strong assumptions on the structural defects. First, the microtwins are isolated from each other (70 nm average separation).

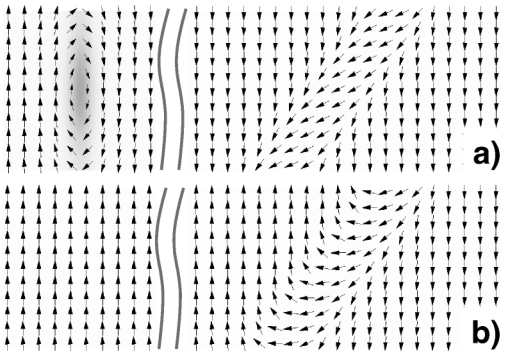

FIG. 2. Cross section of magnetic configurations obtained by micromagnetic simulations on 64 per 512 cells [10 nm (thickness) ×80 nm]. Only the left and right parts are displayed. The dark gray area accounts for magnetization pointing out of the simulation plane. (a) Relaxed configuration for a Bloch wall (left) far away from the microtwin (right). (b) Configuration with the wall pinned on the microtwin.

This allowed us to simulate the interaction of the wall with a single microtwin. Next, the invariance by translation along the microtwins ($\langle 110\rangle$ directions) enables a bidimensional simulation. The micromagnetic simulations have been performed on a 2D box 10 nm thick and 80 nm long by integrating the Landau Lifschitz Gilbert equation using a finite difference code [17]. This box has been divided in a periodic square lattice of 64×512 nodes having a mesh of 0.156 nm. The microtwin is figured out as a volume with a 70.52° tilted magnetocrystalline anisotropy. The simulations presented in Fig. 2 correspond to a 5.4 nm wide defect created by the gliding of 20 dislocations. The demagnetizing field derived from the magnetic configuration inside the simulation box is corrected by the field due to the infinite layer out of the simulation box (saturated up on the left and down on the right); the correction field is calculated analytically. A domain wall [Fig. 2(a)] is introduced in the left part, separating a semi-infinite up domain (left), from a semi-infinite down domain (right). Classical features of the relaxed configuration of the domain wall are the Bloch core, where the magnetization rotates within the plane of the domain wall, and the 2 Néel caps, appeared under the influence of the transverse field created by the two domains. The width of the "free" domain wall (3.7 nm) is comparable to the exchange length (3.2 nm). In the microtwin, the magnetization tilts towards the local anisotropy axis [Fig. 2(a)]. An up field was introduced, and the wall dynamically moved towards the microtwin. The energy cost of the domain wall has been calculated throughout its propagation (low applied field and a strong damping parameter ($\alpha = 1$) made the kinetic energy of the wall negligible). We took into account the dipolar, exchange, and anisotropy energies by reference to a layer comprising a microtwin far away from an abrupt domain wall. When the domain wall gets pinned on the microtwin, major changes arise [Fig. 2(b)]: the wall lays in the plane of the microtwin, the part of the magnetization perpendicular to the {110} plane disappears—as if the Néel cap which first encounters the slanting defect extends over the whole layer thickness—and its width expands up to the one of the microtwin. The wall energy is then strongly reduced (by 80% for a microtwin with 20 partial dislocations). Remarkably, the deepness of this potential well increases linearly with the number of dislocations, up to 20 dislocations [this range comprises 95% of microtwins, Fig. 1(c)]; beyond, it saturates. Hence, the propagating field distribution across the microtwins roughly matches the distribution of the number of constitutive dislocations. To sum it up, the micromagnetic simulations demonstrate that a domain wall is indeed pinned within the energy well provided by the microtwins. Domain wall propagation then occurs across a pseudorectangular lattice of potential wells, located at the interfaces between neighboring cells of up or down magnetization.

Let us now turn towards the large scale magnetic pattern observed during reversal. On most MFM images (up to 128 μm), all features belong to a single reversed domain, implying that reversal started from a single nucleation center, and continued by domain wall propagation (Fig. 3). The mean fractal dimension (1.88) has been extracted from box counting analysis [Fig. 3(c)] [18]. This figure does not change significantly in samples of different thicknesses, having different distributions of the width of the microtwins and hence of the deepness of the pinning energy wells. This remarkable reproducibility will be commented on later. When dominant, the dipolar interactions tend to create a dendritic pattern, that does not display the scale invariance of a fractal configuration [19], the dendrite's width being close to the equilibrium domain size. The scale invariance [Fig. 3(c)] implies that the dipolar field is not a pertinent parameter here, especially at scales much larger than the equilibrium domain size (around 100 nm). This is confirmed by the large unreversed areas observed within the percolating cluster [Figs. 3(a) and 3(b)]. The domain wall propagation process is thus controlled by the structural disorder, that is, according to both micromagnetic simulations and experiments, dominated by the microtwins. We assert that a domain wall crosses a microtwin when the applied field is larger than the propagation field and reverses immediately the entire adjacent cell. But, can we indeed neglect the role of the thermal activation? In other words, are the microtwins exclusively blocking, or passing, at a given field at room temperature? To answer, we relied on time-resolved Kerr microscopy. After saturating the sample in 1.2 T, the long time dynamics was followed: a -0.065 T magnetic field was applied and cancelled each 10 min to perform imaging. The magnetic configuration remained unchanged for hours (Fig. 4). A dramatic event next occurred, that consists in the brutal reversal of and large part of the sample, due to the connection of the reversed domain to a cluster of passing microtwins. The scarcity of such events, likely induced by the thermally activated crossing of a single microtwin, means that the distribution of the pinning energies of the microtwins is large with respect to the thermal activation at room temperature.

We can now account for the large scale magnetic configurations within a simple model. The layer is described as a perfect two-dimensional square lattice, each side of a cell (link) corresponding to one microtwin. The disorder corresponds to a distribution of the propagation fields of the links. At a given applied field, each link is either blocking or nonblocking. With an increasing applied field, clusters of nonblocking bonds are growing. When one of them gets connected to a nucleation site, all the cells of this cluster are reversed. This description constitutes a major step with respect to previous modelings of magnetization reversal in thin layers, in which the disorder coming out from the links between cells was substituted by a distribution of the cell properties [8]. Indeed, the proposed description fits with the percolation theory, allowing analytical predictions. The percolation of the reversed domain occurs when the proportion of nonblocking bonds reaches the percolation threshold ($p = 0.5$ in a square lattice) [18]. Within the experimental time scale, the corresponding field could be named the percolation field, below which the reversed area is negligible

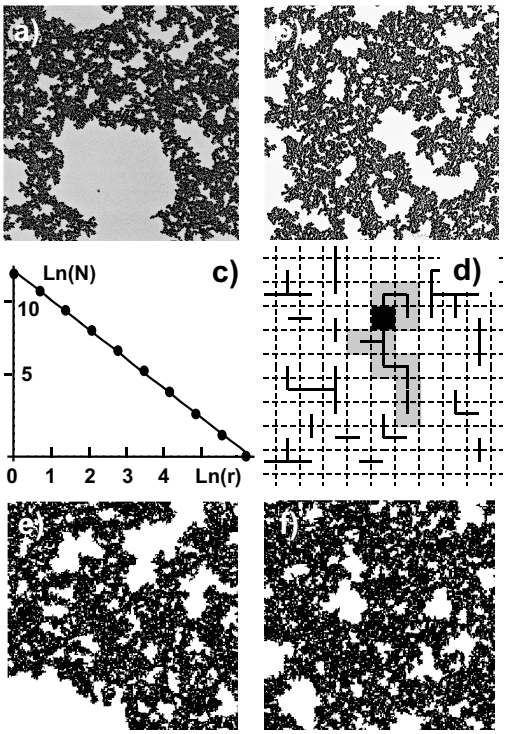

FIG. 3. (a),(b) 64 μm $\times$ 64 μm typical MFM images obtained on FePt(40 nm)/Pt(001) layers: (a) $M/M_S = 0.75$ and fractal dimension $D_{\text{exp}} = 1.87$; (b) $M/M_S = 0.83$ and $D_{\text{exp}} = 1.89$; (c) Box counting analysis of the image (a) with r the counted box size and N the number of boxes containing a part of the reversed domain. (d) Sketch of the grid used for calculations (nucleation center: black cell; passing links: black lines; reversed cells: gray). (e),(f) Patterns simulated at the percolation threshold.

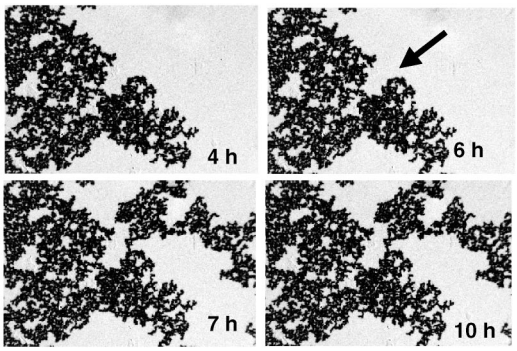

FIG. 4. Magneto-optical polar Kerr images (92 $\times$ 61 μm) of a FePt(40 nm)/Pt(001) layer. The arrow (at 6 h) points to the likely origin of the forthcoming event.

with respect to the sample surface. Experimentally, the percolation corresponds to the first macroscopically observable magnetization reversal event. The Hausendorff-Besicovich fractal Dimension D_{HB} of the domain can be calculated exactly, as the dimension of the infinite cluster at the percolation threshold: $D_{HB} = d - \beta/\nu = 91/48 = 1.896$, with $d = 2$ being the dimension of the lattice, β and ν being the critical exponents for a bidimensional system [18]. These exponents being universal, the fractal dimension does not depend on the details of the structure of the lattice. This gives ground to the approximation made by considering a square lattice of microtwins: whatever the exact structure, whatever the number of bonds between a cell and the neighboring ones, the fractal dimension will be the same. In addition, it explains why, even if the sample thickness (hence, the distribution of the propagation fields) is changed, we measured unchanged fractal dimensions. Interestingly, in Ising-like models with random bonds or random fields, a transition between compact and percolationlike growth appears, depending on the strength and distribution of the disorder [20]. In our case, the amplitude of the disorder is large with respect to thermal activation and to local changes in demagnetizing field, thus the disorder is the sole parameter governing the domain growth, which always corresponds to a percolation phenomenon. From MFM images, we get $D_{EXP} = 1.88$, a value remarkably close to the theoretical one $D_{HB} = 1.896$. To allow for a qualitative comparison, numerical simulations of the top view magnetic pattern were made on the basis of this model. One reversed cell (nucleation) was introduced at the center of a 1024×1024 lattice. Blocking or nonblocking bonds were randomly distributed [Fig. 3(d)]. Images were retained at the percolation threshold ($p = 0.5$), when the cluster was in contact with the four sides of the box. To limit finite size effects, only the center part of the images (512×512) is displayed. These numerical images [Figs. 3(e) and 3(f)] are very similar to the experimental ones [Figs. 3(a) and 3(b)]. Obviously, the quantitative agreement between a simple analytical description and the experimental data found limits at small and large scales. These are inherent to the fractality, as a real system cannot be unendingly scale invariant. At low scale, the dimension and shape anisotropy of the microtwin lattice are apparent [Fig. 1(d)]. At very large scales, there may be enough nucleation centers to lead to more homogeneous and thus nonfractal patterns.

To sum it up, our study revealed new features of domain wall propagation within strongly disordered media, in the case of correlated defects. Unique features of the FePt/Pt(001) thin layers are the well-identified strain relaxation defects, the microtwins, that control the domain wall propagation. In contrast with previous studies of weak disorder in thin films, the energy gain associated with domain wall pinning on the microtwin is large with respect to the domain wall energy. Hence, these very thin linear defects can efficiently localize the domain wall at room temperature, modifying dramatically its shape at small scales. However, the local "deroughening" of the domain wall, when aligned on the defect, does not prevent the expression of disorder at larger scales. Indeed, the propagation field (and the related waiting time) on a microtwin varies from defect to defect, thereby leading from a single nucleation event to the appearance of a fractal domain during magnetization reversal. The system can be modeled by a periodic lattice of links, i.e., each links between two cells, allowing or blocking the propagation of the domain wall from a cell to the neighboring one. This approach differs from previous models of similar processes, usually based on Monte Carlo simulations where, e.g., the disorder related to grains boundaries was figured out by distributions of the cells themselves [8,19]. It allows for analytical modeling and successful quantitative predictions by using the percolation theory. Domain wall propagation studies are also driven by applications. Most approaches of ultrahigh density media target patterned systems, where magnetic dots are separated by voids [21] or nonferromagnetic materials [22]. In this regard, even if the synthesis of appropriate samples would be challenging, the efficient pinning of domain walls by nanometer scale, ferromagnetic anisotropy defects opens new and promising perspectives.

*Corresponding author.
Email address: ysamson@cea.fr

[1] N. Martys *et al.*, Phys. Rev. Lett. **66**, 1058 (1991).
[2] R. Surdeanu *et al.*, Phys. Rev. Lett. **83**, 2054 (1999).
[3] B. E. Bernacki *et al.*, J. Appl. Phys. **69**, 4960 (1991).
[4] G.V. Sayko *et al.*, IEEE Trans. Magn. **28**, 2931 (1992).
[5] A. Kirilyuk *et al.*, J. Magn. Magn. Mater. **171**, 45 (1997).
[6] B. S. Han *et al.*, Phys. Rev. B **66**, 014433 (2002).
[7] A. Lyberatos, J. Magn. Magn. Mater. **186**, 248 (1998).
[8] J. Ferré, *Spin Dynamics in Confined Magnetic Structures* (Springer-Verlag, Berlin, 2002), Chap. 5.
[9] Sug-Bong-Choe *et al.*, IEEE Trans. Magn. **36**, 3167 (2000).
[10] A. Lyberatos *et al.*, J. Phys. D **33**, 1060 (2000).
[11] J. Ferré *et al.*, Phys. Rev. B **55**, 15 092 (1997).
[12] U. Nowak *et al.*, Phys. Rev. B **54**, 13 017 (1996).
[13] D. Halley, Ph.D. thesis, Université de Grenoble (France), 2001.
[14] D. Halley *et al.*, Phys. Rev. B **65**, 205408 (2002).
[15] J. P. Attane *et al.*, Appl. Phys. Lett. **79**, 794 (2001).
[16] P. Haibach *et al.*, Phys. Rev. Lett. **84**, 1312 (2000).
[17] J. C. Toussaint *et al.*, Comput. Mater. Sci. **24**, 175 (2002).
[18] A. Bunde *et al.*, *Fractal and Disordered Systems* (Springer-Verlag, Berlin, 1991), Chap. 2.
[19] A. Lyberatos, J. Phys. D **33**, 117(R) (2000).
[20] H. Ji *et al.*, Phys. Rev. A **44**, 2538 (1991).
[21] W. Wu *et al.*, J. Vac. Sci. Technol. B **16**, 3825 (1998).
[22] C. Chappert *et al.*, Science **280**, 1919 (1998).